


Charge-Transfer Dynamics in OLEDs with Coexisting Electroplex and Exciton States

Yaru Ning, Xi Zhao, Fengjiao Wu, Yuting Wu, Jing Chen, Fuxian Wei, Huiyao Wang, Xiaoli Chen, and Zuhong Xiong^{✉*}

Chongqing Key Laboratory of Micro&Nano Structure Optoelectronics, School of Physical Science and Technology, Southwest University, Chongqing 400715, China

 (Received 1 December 2022; revised 10 May 2023; accepted 18 May 2023; published 16 June 2023)

The reverse intersystem-crossing (RISC) channels from triplet to singlet charge-transfer states (such as exciplex or electroplex states) frequently occur in donor:acceptor heterojunction organic light-emitting diodes (OLEDs) to achieve high external quantum efficiency. Although exciplexes have been extensively investigated, there are few reports on the physical microscopic processes for electroplex-based devices. Herein, three kinds of donor:acceptor heterojunction OLEDs are fabricated: two coexisting electroplex and exciton devices and one pure exciplex-based device. Amazingly, via the fingerprint magneto-electroluminescence measurement at room temperature, we observe an abnormal current-dependent RISC, which is enhanced with increasing bias current (I) in the coexisting electroplex and exciton but electroplex-dominated device; the conversion from ISC to RISC in the coexisting electroplex and exciton but exciton-dominated device; and only the normal I -dependent ISC, which weakens with increasing I in the pure exciplex-based device. This is because low-energy-triplet electroplexes are well confined by the high triplet energies of electron donors and acceptors, promoting the occurrence of the RISC process in electroplexes, and Dexter energy transfer from triplet excitons to triplet electroplexes enhances the RISC process with increasing I , causing the abnormal I -dependent RISC and the conversion from ISC to RISC. Moreover, as the operational temperature rises from 10 to 300 K, these two coexisting electroplex and exciton devices present the conversion from ISC to RISC at different temperatures, but the pure exciplex-based device shows only the normal temperature-dependent ISC, which is enhanced with increasing temperature. This is because the RISC channel is an endothermic process and temperature-dependent electroluminescence measurements show that the electroplex emission weakens as the temperature is reduced, causing the weakened RISC process and even the presence of the ISC process at low temperature. These experimental results demonstrate that the electroplex emission plays an important role in the occurrence of strong RISC processes. Our work deepens our microscopic understanding of the charge-transfer states in donor:acceptor heterojunction devices but also paves the way for utilizing electroplex states to design highly efficient OLEDs.

DOI: [10.1103/PhysRevApplied.19.064055](https://doi.org/10.1103/PhysRevApplied.19.064055)

I. INTRODUCTION

Exciplex- and electroplex-based organic light-emitting diodes (OLEDs) have attracted extensive attention because they can harvest singlet and triplet charge-transfer states (CT_1 and CT_3 , respectively) by the reverse intersystem-crossing (RISC, $CT_1 \leftarrow CT_3$) process to raise the external quantum efficiency (EQE) of OLEDs [1–3]. Moreover, using magneto-electroluminescence (MEL) as a fingerprint probing technique, Zhao *et al.* observed the RISC process of 4,4',4''-tris(carbazol-9-yl)triphenylamine (TCTA):2,4,6-tris[3-(diphenylphosphinyl)phenyl]-1,3,5-triazine (PO-T2T) exciplexes in balanced OLEDs [4]. In recent years, much scientific research has mainly

focused on the RISC process and the device performances from exciplex states [5–7]. One reason is that the exciplex emission can be observed in both electroluminescence (EL) and photoluminescence (PL) spectra, but the electroplex emission occurs only under an external electric field, i.e., the electroplex emission cannot happen under photoexcitation [8,9]. Like the exciplex, the electroplex can be used to fabricate stable white OLEDs or as a host for fluorescence, phosphorescence, and thermally activated delayed fluorescence (TADF) [3,10–12]. For example, Tang *et al.* fabricated a warm-white OLED with a maximum EQE of 13.7% via utilizing a broad interfacial electroplex emission [12]. Yun *et al.* developed a bipolar host, 3-(4-(9H-carbazol-9-yl)-6-(3-(triphenylsilyl)phenyl)-1,3,5-triazin-2-yl)benzotrile (SiTCNCz), with the TADF property and obtained a high

*zhxiong@swu.edu.cn

EQE of 20.4% from a 3,3'-di(9*H*-carbazol-9-yl)biphenyl (mCBP):SiTCNCz electroplex-based deep blue phosphorescent OLED through dual triplet-exciton upconverting channels [3]. Although both exciplex and electroplex states show redshifted and broad EL spectra compared with the PL spectra of their monomers, electroplex states often possess lower energies and smaller splitting energies (ΔE_{ST}) between CT_1 and CT_3 than exciplexes [13,14]. Accordingly, electroplex states are more conducive to the occurrence of the RISC process than exciplexes because the triplet-exciton energies of donor and acceptor molecules are easily higher than those of electroplex states, and electroplex states can be well confined within the emitting layer without any energy-loss channel. That is, to some extent, an electroplex can be an ideal alternative to an exciplex. Nevertheless, many microscopic dynamic processes of electroplex-based OLEDs are still unclear because the electroplex states are rarer than exciplexes.

Herein, using the donor:acceptor mixing system as an emissive layer, three kinds of donor:acceptor heterojunction OLEDs are fabricated: a coexisting electroplex and exciton but electroplex-dominated device (hereafter referred to as device A or the electroplex-dominated device), a coexisting electroplex and exciton but exciton-dominated device (device B or the exciton-dominated device), and a pure exciplex-based device as a reference one (device C or the exciplex-only device). Devices A–C have light-emission layers of mCBP:Bphen, mCBP:TPBi, and *m*-MTDATA:Bphen, respectively. Here, Bphen, TPBi, and *m*-MTDATA are the abbreviations of 4,7-diphenyl-1,10-phenanthroline, 1,3,5-tris(*N*-phenyl-benzimidazol-2-yl) benzene, and 4,4',4''-tris(*N*-3-methylphenyl-*N*-phenylamino)triphenylamine, respectively. The MEL responses of these three devices are measured at a range of bias currents (I) and various operational temperatures, because MEL can be utilized as an effective detection tool to visualize various evolution channels occurring in devices [15–17], such as RISC and ISC of charge-transfer states or polaron pairs (see Fig. S1 and its relevant interpretation within the Supplemental Material [18]). Intriguingly, abundant physical behaviors of I -dependent MEL curves can be observed in these three devices at room temperature (300 K). Specifically, electroplex-dominated device A presents the fingerprint MEL traces of a magnetic-field- (B) mediated RISC process at all I and the MEL magnitudes are enhanced with increasing I (i.e., abnormal I -dependent RISC process), while the MEL traces in the exciton-dominated device B show the conversion from B -mediated ISC to RISC processes with increasing I . Contrarily, the exciplex-only device C shows the fingerprint MEL curves of B -mediated ISC process at each I and the MEL magnitudes decrease with increasing I (i.e., normal I -dependent ISC process). Clearly, these emissive states (including electroplexes, excitons, and exciplexes) of devices have remarkable effects on the different MEL curves and the intensity of

electroplex emission relative to exciton emission determines whether the RISC process or the ISC process is dominant. This is because the low-energy triplet electroplex is well confined in the emissive layer by the high-energy triplet excitons of electron donors and acceptors, promoting the occurrence of the RISC process. Moreover, the effective Dexter-energy-transfer (DET) channel from triplet excitons to triplet electroplexes causes abnormal I dependence of RISC processes from electroplex states. Specifically, the DET channels from triplet excitons to triplet electroplexes ($T_{1,Bphen} \rightarrow CT_{3,mCBP:Bphen}$, $T_{1,TPBi} \rightarrow CT_{3,mCBP:TPBi}$) can effectively occur in devices A and B at large I , and are enhanced with increasing I . The occurrence of DET increases the number of CT_3 states and RISC processes from mCBP:Bphen and mCBP:TPBi, thereby leading to the abnormal I dependence of the RISC process and the conversion from ISC to RISC processes with increasing I in electroplex- and exciton-dominated devices A and B, respectively. Furthermore, as the operational temperature rises from 10 to 300 K, these two coexisting electroplex and exciton devices A and B display the conversion of characteristic MEL responses from the B -mediated ISC to RISC processes, but exciplex-only device C displays the MEL traces of the ISC process at all operational temperatures and the MEL magnitudes increase as the temperature rises. This is because the RISC process is an endothermic process and temperature-dependent EL spectra show that electroplex emission weakens with decreasing temperature, and thus, the RISC process weakens with decreasing temperature and even the ISC process occurs at low temperature. Our research work deepens our physical understanding of charge-transfer states in donor:acceptor heterojunction devices but also has important implications for employing electroplex states to fabricate high-efficiency OLEDs.

II. EXPERIMENTAL SECTION

In this study, all donor:acceptor heterojunction OLEDs are fabricated with the following device structure [see Fig. S2(a) within the Supplemental Material [18]]: indium tin oxide (ITO)/poly(3,4-ethylenedioxythiophene):poly(styrenesulfonate) (PEDOT:PSS)(40 nm)/1,1-bis[(di-4-tolylamino)phenyl]cyclohexane (TAPC)(40 nm)/donor (20 nm)/donor:acceptor(1:1, 50 nm)/acceptor(50 nm)/lithium fluoride (LiF)(1 nm)/Al(100 nm). Among them, two devices are obtained by combining the mCBP donor with Bphen or TPBi acceptors, and these are named devices A and B, respectively. For comparison, pure exciplex-type device C based on *m*-MTDATA:Bphen is also prepared. Herein, ITO/PEDOT:PSS is a composite anode, LiF/Al is a composite cathode, and TAPC is used as a hole-transporting layer to reduce the hole-injection barrier. During the preparation of samples, PEDOT:PSS is spin-coated onto well-cleaned ITO-patterned glass substrates followed by annealing at 120 °C for 10 min in

air. Other organic functional layers are grown using the deposition technique of a multiple-source organic molecular beam under high vacuum ($\sim 10^{-5}$ Pa). The active area of the device is 2×3 mm².

After device fabrication, the samples are mounted on the cold finger of a closed-cycle cryostat (Janis CCS-350S) that is located between the poles of an electromagnet (Lakeshore EM647). The magnitude of an external B is measured using the Hall probe of a gaussmeter placed close to the samples. The applied bias voltage is supplied by a Keithley 2400 source meter, and the relative light-emissive brightness of devices is determined using a magnetic insensitive silicon photodetector connected with a Keithley 2000 multimeter and recorded by a personal computer. The device operational temperatures are set with the use of a temperature controller (Lakeshore 331). In addition, the EL spectra of devices are measured with a SpectraPro-2300i spectrometer (Princeton Instruments). The stable PL spectra and transient PL decays of pristine and blend films are measured with an Edinburgh fluorescence spectrometer (FLS 1000).

III. RESULTS AND DISCUSSION

A. Analyses of the emission behaviors of mCBP:Bphen, mCBP:TPBi, and *m*-MTDATA:Bphen under optical and electrical excitation

To investigate the combined effects of different electron donors and acceptors with various highest occupied

molecular orbital (HOMO) and lowest unoccupied molecular orbital (LUMO) levels on device emission species, a series of bulk heterojunction OLEDs are fabricated (see Sec. II). Among them, the selected donor materials are mCBP and *m*-MTDATA, and the acceptor materials are Bphen and TPBi; their molecular structures are shown in Fig. S2(b) within the Supplemental Material [18]. Figure 1 displays schematic diagrams of LUMO and HOMO energy levels in the emitting layers and the formation processes of exciton, electroplex, and exciplex states. When the mCBP:Bphen film is excited by a xenon lamp with a wavelength of 280 nm (corresponding to an excited photon energy of 4.43 eV), both the mCBP donor and Bphen acceptor are excited to generate singlet excitons, according to the energy differences (3.7 and 3.4 eV) between the LUMO and HOMO levels of mCBP and Bphen molecules [19,20]. Notably, the singlet-exciton energy of mCBP is higher than that of Bphen; thus, only the Bphen exciton emission (PL₁) can be observed after the Förster-resonance energy transfer of singlet excitons from mCBP to Bphen molecules under optical excitation. However, when an external bias voltage is applied to device A, based on mCBP:Bphen, because the energy-level offsets of the LUMO and HOMO between mCBP and Bphen molecules are 0.6 and 0.3 eV, respectively, the majority of injected electrons accumulate on the LUMO level of Bphen and partially injected holes reside on the HOMO level of mCBP, so then electrons recombine with holes to form the electroplex (EL₁), which is not observed under

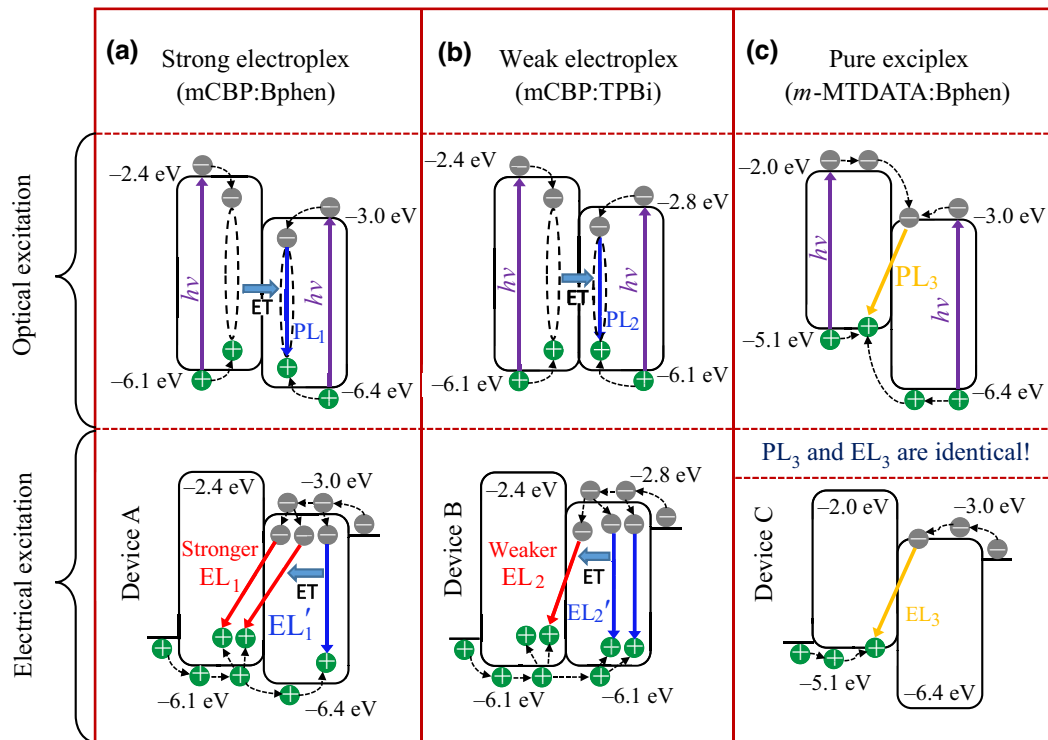


FIG. 1. Emission behaviors of (a) mCBP:Bphen, (b) mCBP:TPBi, and (c) *m*-MTDATA:Bphen under optical and electrical excitations.

photoexcitation. Meanwhile, a minority of holes can overcome the energy barrier to reach the HOMO level of Bphen due to the small energy-level offset between the HOMOs of mCBP and Bphen. Thus, these injected holes can recombine with electrons on the LUMO of Bphen to generate Bphen's exciton emission (EL_1'). Therefore, both electroplex states of mCBP:Bphen and Bphen excitons are simultaneously produced in device A under electrical excitation, but the electroplex quantity is greater than that of the exciton (i.e., $EL_1 > EL_1'$), i.e., device A is the coexisting electroplex and exciton but electroplex-dominated device.

When the TPBi [21] acceptor with the same HOMO level as that of mCBP [19] is used instead of Bphen, the emission behavior of the mCBP:TPBi codeposited film under optical excitation is similar to that of the mCBP:Bphen codeposited film, forming a low-energy TPBi exciton emission (PL_2) compared to that of the mCBP exciton. Nevertheless, due to the exactly equal HOMO levels of mCBP and TPBi, more holes will pass through mCBP to reach the TPBi HOMO levels in device B under the action of an external bias voltage. In this case, a large number of electrons at the LUMO level of TPBi preferentially recombine with holes at the HOMO level of TPBi to generate strong excitons on TPBi acceptor molecules (EL_2'). Additionally, minority residual electrons recombine with holes at the HOMO level of mCBP, resulting in the weak electroplex emission (EL_2) of mCBP:TPBi. This means the presence

of more excitons than electroplexes (i.e., $EL_2 < EL_2'$) in device B under electrical excitation, i.e., device B is the coexisting electroplex and exciton but exciton-dominated device.

To increase the HOMO-level difference between the donor and acceptor, the *m*-MTDATA donor with the HOMO level of 5.1 eV [20] is used instead of mCBP. In this case, regardless of optical or electrical excitation, the huge energy-level offsets of the LUMO and HOMO levels between *m*-MTDATA and Bphen molecules lead to the accumulation of electrons at the LUMO level of Bphen and holes at the HOMO level of *m*-MTDATA, thereby the radiative transition from electrons to holes forms only exciplex emissions (i.e., PL_3 and EL_3 are identical). Thus, the pure exciplex emission is observed from *m*-MTDATA:Bphen in device C. Notably, these above reasonable analyses for the emission behaviors of devices A–C are verified by their PL and EL spectra in the following section.

B. Photoelectric properties and *I*-dependent MEL responses of devices A–C at 300 K

The normalized EL spectra of devices A–C and the normalized PL spectra of the corresponding donor:acceptor blend films and each monomer material are displayed in Figs. 2(a)–2(c), respectively. As can be seen from Fig. 2(a), the PL peak of the mCBP:Bphen codeposited film (402 nm) is almost identical to that of the Bphen

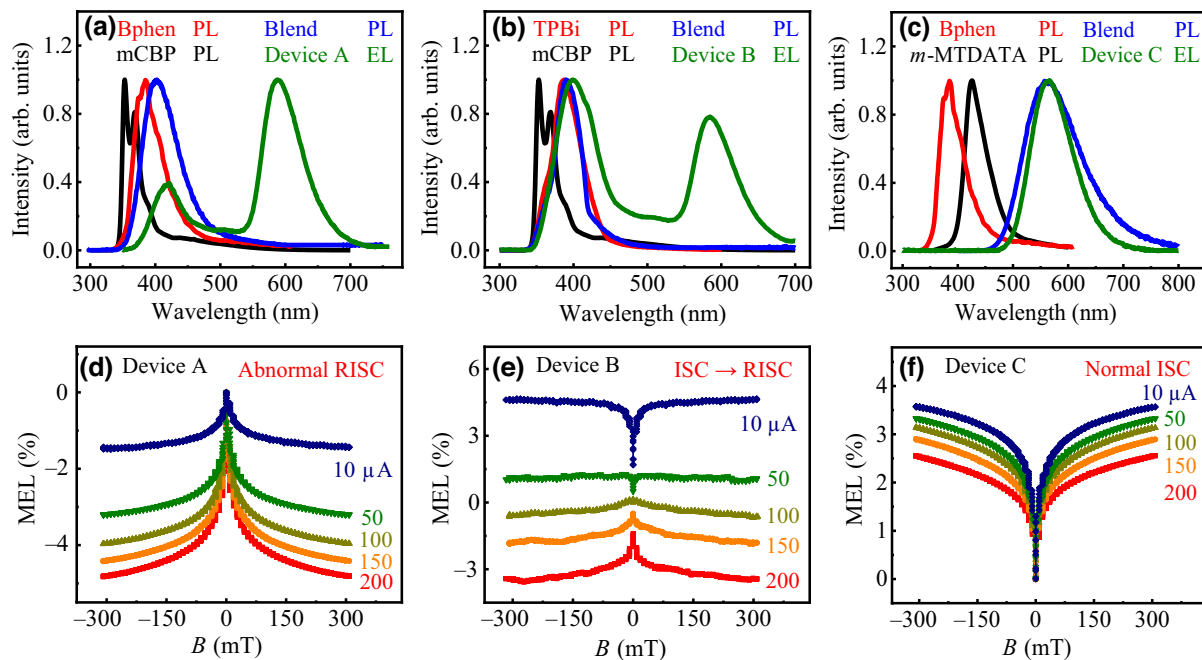


FIG. 2. (a) Normalized PL spectra of mCBP, Bphen, and mCBP:Bphen films and normalized EL spectrum of device A. (b) Normalized PL spectra of mCBP, TPBi, and mCBP:TPBi films and normalized EL spectrum of device B. (c) Normalized PL spectra of *m*-MTDATA, Bphen, and *m*-MTDATA:Bphen films and normalized EL spectrum of device C. (d)–(f) *I*-Dependent MEL curves of devices A–C at 300 K.

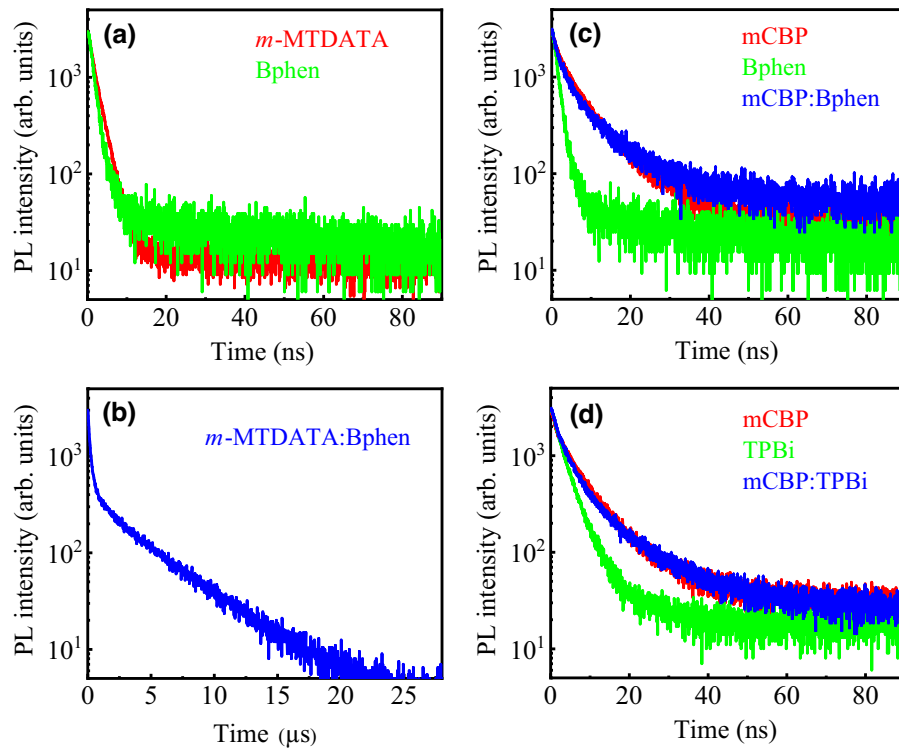


FIG. 3. Transient PL decay profiles of (a) *m*-MTDATA and Bphen pristine films; (b) *m*-MTDATA:Bphen blend film; (c) mCBP, Bphen, and mCBP:Bphen films; and (d) mCBP, TPBi, and mCBP:TPBi films.

film (385 nm), suggesting that only the Bphen exciton emission exists in mCBP:Bphen under optical excitation, which can be also proved in the transient PL decay of this blend film depicted in Fig. 3(c). Interestingly, besides the Bphen exciton emission at around 400 nm, device A has another main EL spectrum peak at 588 nm, and this main peak is redshifted compared with the PL peaks of the constituent pristine materials. These results indicate that a new species called an electropex or electromer is formed in device A under electrical excitation, because these emissions can only be observed in the EL spectra [10–14,22]. From the EL and PL spectra displayed in Fig. 2(b), the TPBi exciton has a characteristic emission peak at 387 nm, which is almost identical to the emission peak (390 nm) of the mCBP:TPBi blend film. However, we observe double-emissive states in the EL spectrum of device B, with peaks at 410 and 590 nm. Due to the absence of the PL peak at 590 nm in the mCBP:TPBi blend film, the TPBi exciton and electropex or electromer coexist in device B. Nevertheless, we rule out electromer emissions of mCBP, Bphen, or TPBi in devices A and B. This is because carbazole-based mCBP has a strong electron-donating ability [23], when mCBP is combined with Bphen or TPBi that possesses an electron-accepting ability, exciplex or electropex formation is preferential. Meanwhile, the donor:acceptor mixing ratios of the emissive layers in our fabricated devices are 1:1. This indicates that the donor (or acceptor)

molecules are spatially well separated from each other, and the molecular spacing distances are relatively large. However, the electromer is defined as the two same intermolecular species with a distance of 0.3–0.4 nm [24] and exists only during electrical excitation, which demands very close molecular distances. Obviously, our device structures are disadvantageous for electromer formation. In fact, the intensity of the electromer-emission bands in most bulk heterojunction devices involving multiple emissive states is usually weak [24,25], whereas the peak located at around 580 nm dominates over the exciton emission in device A and is comparable to the exciton emission in device B. In contrast, the electromer-emission bands often present obvious redshifts with increasing device *I* [24], but our devices A and B do not show any peak shifts, as displayed in Fig. S3 within the Supplemental Material [18]. These experimental results rule out any electromer formation in devices A and B. In passing, as reported in the literature [22], the electromer emission of CBP peaks at 625 nm, and mCBP has the same HOMO and LUMO energy levels as those of CBP, thus mCBP should have a similar electromer-emission peak at around 625 nm. Therefore, the emission components peaking at 580–590 nm in devices A and B are mCBP:Bphen and mCBP:TPBi electropexes rather than electromers of mCBP, Bphen, or TPBi.

Furthermore, note that the electropex emission is much larger than the Bphen exciton emission in device A, while

the EL spectrum of device B is dominated by the TPBi exciton emission. These phenomena can be supported by the emission behaviors of mCBP:Bphen and mCBP:TPBi under electrical excitation, as shown in Fig. 1. Meanwhile, we find that the electroplex emissions in Figs. 2(a) and 2(b) are significantly redshifted compared with those from excitons in their donor and acceptor counterparts. As reported in the literature [8], an electroplex is formed by the cross-recombination of a hole in the HOMO from donor molecules (D^+) and an electron in the LUMO from acceptor molecules (A^-), while an exciton is the direct transition from an electron in the LUMO to a hole in the HOMO of the single molecule. The electroplex energy is determined by the HOMO-LUMO energy-level difference between donor and acceptor molecules and the electron-hole binding energy [8], whereas the exciton energy is dependent on the HOMO-LUMO difference of individual constituent molecules. Since the HOMO-LUMO differences between mCBP and Bphen or TPBi molecules are smaller than those of individual donor and acceptor molecules, the energy of an electroplex is lower than that of the constituent molecules. Significantly, mCBP:Bphen and mCBP:TPBi electroplexes have similar emission wavelengths. Although the HOMO-LUMO energy differences of devices A and B are 3.1 and 3.3 eV, respectively, their larger electron-hole binding energies, due to the strong electron-donating ability of mCBP, can result in little difference in the emission wavelengths peaking at 580–590 nm for devices A and B. On the other hand, the band-gap difference between devices A and B is only 0.2 eV; such a small energy difference is acceptable for the observed similar emission wavelengths provided that electroplex states in devices A and B have small binding-energy differences (0.2 eV).

In contrast, the EL spectrum of device C from Fig. 2(c) reflects a different emissive peak from those of devices A and B. Specifically, the EL spectrum of device C almost completely coincides with the PL spectrum of the *m*-MTDATA:Bphen codeposited film, and the emission peaking at 567 nm, which corresponds to the HOMO-LUMO energy-level difference (2.1 eV) of *m*-MTDATA and Bphen molecules, is significantly redshifted and broadened compared with the PL emission peaks of *m*-MTDATA (426 nm) and Bphen (385 nm), respectively. This confirms effective exciplex formation, which occurs under both optical and electrical excitation. Clearly, the experimental results shown in Figs. 2(a)–2(c) are in good agreement with the emissive behavior analyzed in Fig. 1. Due to various device structures and energy levels, the EL spectra of these three devices show multicomponent emissions containing electroplex and exciton states (devices A and B) and pure exciplex emissions (device C). For the systems with coexisting excitons and electroplexes, little research has focused on their internal microscopic mechanisms. Fortunately, the noncontact and nondestructive fingerprint

MEL traces occurring in OLEDs can be used to visualize these microscopic processes [15–17]. Hence, MEL curves from devices A–C are systematically investigated as follows. The main purpose of the MEL measurement for device C with exciplex-only emissions is used to compare exciplexes and electroplexes to determine the microscopic mechanisms of the electroplex states.

Figures 2(d)–2(f) show the I -dependent MEL curves of devices A–C at 300 K, respectively. The MEL is usually defined as $\text{MEL} = (\Delta\text{EL})/\text{EL} = [\text{EL}(B) - \text{EL}(0)]/\text{EL}(0) \times 100\%$, where $\text{EL}(B)$ and $\text{EL}(0)$ are the EL intensities with and without an external B , respectively. As can be seen from Figs. 2(d) and 2(f), devices A and C have completely opposite MEL traces. Specifically, the MEL curves of device A first rapidly reduce (i.e., the upright Lorentzian-type line shape) in the range of $|B| \leq 9$ mT (low-field effects, LFEs) followed by the slow decrease in the range of $9 \text{ mT} < |B| \leq 300$ mT (high-field effects, HFEs) at each I . Nevertheless, the MEL traces of device C present rapidly increasing LFEs (i.e., the inverted Lorentzian-type line shape) and slowly increasing HFEs at all I . As reported in the literature [4,16], sharply decreasing (or increasing) LFEs are usually attributed to the B -mediated RISC (or ISC) process of intermolecular polaron pairs or charge-transfer states, and the flat tendency of HFEs is because the suppression of RISC or ISC processes by B reaches saturation (see Fig. S1 and its detailed explanation within the Supplemental Material [18]). It is worth mentioning that, as I increases from 10 to 200 μA , the amplitude values of the MEL curves in devices A and C at 9 mT monotonically increase and decrease; these are characteristic of the abnormal I -dependent RISC process and the normal I -dependent ISC process, respectively [26,27]. Interestingly, the LFEs of MEL responses in device B display a gradual change from ISC to RISC processes as I rises. Combined with the EL spectra of these three devices in Figs. 2(a)–2(c), it can be concluded that these different MEL line shapes have one-to-one corresponding EL spectra. That is, the MEL traces of device A, with electroplex-dominated double-emissive states, present the abnormal I -dependent RISC process; the MEL traces of device B, with exciton-governed double-emissive states, show the conversion from ISC to RISC processes with increasing I ; and the MEL curves of device C, with pure exciplex emissions, depict the normal I -dependent ISC process. Notably, when the electroplex is present in the devices, the RISC process is more likely to occur. Therefore, we speculate that the electroplex emission is the main reason for the occurrence of the RISC process. Furthermore, as can be seen from Figs. 2(d)–2(f), there is no obvious change in the HFEs of the MEL responses for these three devices, although their LFEs show abundant behaviors. Accordingly, these LFEs of these three devices are the focus of our work. Thus, we discuss only the physical microscopic mechanisms reflected by the LFEs of all MEL curves, and

the specific microscopic evolution channels are analyzed in Sec. III E.

In addition, the EQE values of these three devices are given in Fig. S4 within the Supplemental Material [18] as a function of luminance. As can be seen, the EQE maxima of devices A–C are 1.85%, 0.72%, and 5.26%, respectively. Notably, although both devices A and B display relatively low EQE values compared with that of exciplex-based device C, electroplex-dominated device A has a much larger EQE than that of exciton-dominated device B. This can be attributed to the presence of a stronger RISC process from electroplex states in device A than in device B. As reported in the literature [28], the EQE of an OLED can be expressed as $\text{EQE} = \gamma \eta_r \eta_{\text{PL}} \eta_{\text{out}}$, where γ is the charge-carrier balance factor, η_r is the fraction of radiative excitons, η_{PL} is the photoluminescence quantum yield (PLQY) of an emitter, and η_{out} is the optical outcoupling efficiency of the device. Clearly, these parameters are closely related to the device structures and materials selected. Due to the large PLQY of the *m*-MTDATA:Bphen film, a high EQE is usually obtained in typical exciplex-based device C [29]. For devices A and B, although the utilization of triplet excitons, as reflected by their MEL curves, is high, i.e., η_r has a relatively large value, an unbalanced charge-carrier injection (small γ) and low PLQYs lead to their low EQEs. This indicates that the structural design and functional layer thickness of devices A and B need to be further optimized, and related work for improving the electroplex-based device efficiency is still under investigation.

C. Transient PL characteristics of a series of pristine and blend films

Figures 3(a)–3(d) depict transient PL decay profiles of a series of pristine and blend films at 300 K. Their relevant fitting data obtained from a double-exponential decay model, $R(t) = B_1 \exp(-t/\tau_1) + B_2 \exp(-t/\tau_2)$, are listed in Table S1 within the Supplemental Material [18], where t is the transient time, and τ_1 and τ_2 are the relaxation lifetimes of the first and second components, respectively. It is clearly found that the transient PL decay curve of the *m*-MTDATA:Bphen film [Fig. 3(b)] displays a double-exponential decay, and prompt and delayed fluorescence lifetimes of 0.196 and 4.09 μs can be observed, which are obviously prolonged lifetimes ($\sim\mu\text{s}$) relative to the lifetimes ($\sim\text{ns}$) of *m*-MTDATA and Bphen [Fig. 3(a)]. This can be ascribed to the occurrence of RISC processes of exciplexes in the blend film of *m*-MTDATA:Bphen. However, notably, device C, based on *m*-MTDATA:Bphen, shows MEL responses of the net *B*-mediated ISC process. This is because MEL is an overlapping effect of the ISC of polaron pairs and the RISC of charge-transfer states, and the ISC is stronger than the RISC. In contrast, the transient PL profiles of mCBP:Bphen (with the Bphen exciton

emission) [Fig. 3(c)] and mCBP:TPBi blend films (with the TPBi exciton emission) [Fig. 3(d)] are similar to that of the mCBP neat film, and they all exhibit decay lifetimes of nearly a few nanoseconds, which means the existence of only prompt fluorescence. Obviously, when each component is excited in the blend film under optical excitation and there is energy transfer from one film to another, the resultant fluorescence decay of the blend film is determined by the transient PL of the monomer material with slower decay (longer lifetime) behavior. Because the efficient energy-transfer processes from mCBP to Bphen or TPBi occur in the mCBP:Bphen or mCBP:TPBi films, and the fluorescence decay of mCBP is slower than that of Bphen or TPBi, the observed transient PL curves of the blend films are close to that of mCBP rather than Bphen or TPBi, which exactly reflects the efficient energy-transfer processes existing in the blend films. In passing, the electroplex states cannot occur in the optical blend films of mCBP:Bphen or mCBP:TPBi. Thus, these above results reveal the absence of exciplexes and the presence of excitons in both mCBP:Bphen and mCBP:TPBi films, which is in excellent agreement with the analyses of the PL and EL spectra discussed in Sec. III B.

D. EL spectra and MEL curves of devices A and B with a 520-nm high-pass filter

From the MEL curves displayed in Figs. 2(d)–2(f), the net ISC process is obtained in device C, while the RISC processes are observed in devices A and B. Therefore, electroplex states play a key role in the occurrence strength of RISC processes in devices A and B. On the basis of the above analysis, a high-pass filter with a minimum transmissibility wavelength of 520 nm is used in the EL and MEL measurements for devices A and B at 300 K. The EL spectra with and without the application of this high-pass filter for devices A and B are displayed in Figs. 4(a) and 4(b), respectively. When this filter is applied, the exciton emission (around 400 nm) will not pass through the filter and only electroplex emissions (peaking at 588 nm) are detected. In this case, the filtered MEL traces for devices A and B are shown in Figs. 4(c) and 4(d), respectively. Surprisingly, the filtered LFEs from devices A and B present the abnormal *I*-dependent RISC process and the enhanced MEL magnitudes, compared with the unfiltered LFEs. Particularly, with the application of the 520-nm high-pass filter, the MEL curves from device B change from the conversion from ISC to RISC to the abnormal *I*-dependent RISC process, which is enhanced with increasing *I*. The reason behind this amazing change may be related to the great variation of exciton quantities in device B. When the exciton-dominated emission is filtered, only the electroplex emission is left. The ISC process originating from *B*-mediated polaron-pair states, as the precursors for these dominating excitons, will be

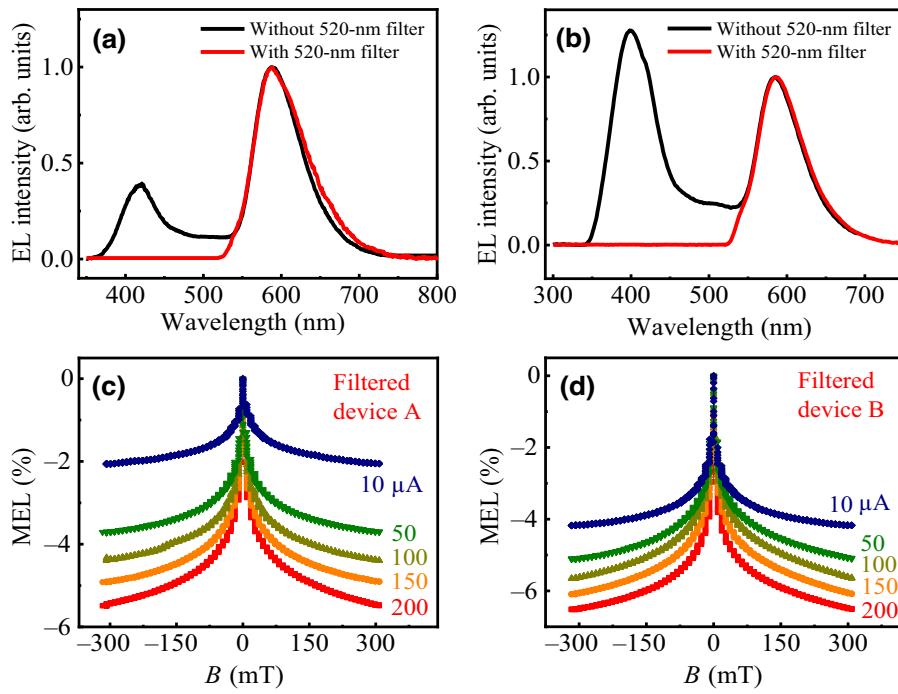


FIG. 4. (a),(b) Normalized EL spectra with and without the 520-nm high-pass filter for devices A and B, respectively. (c),(d) I -Dependent MEL curves of devices A and B with a 520-nm high-pass filter, respectively.

suppressed in the MEL measurements. This leads to the greatly enhanced RISC process because MEL is an overlapping effect when there are several B -sensitive channels (here, ISC and RISC for LFEs) and ISC and RISC have opposite MEL traces. Notably, the magnitudes of the filtered LFEs for device B are larger than those for device A; this is in excellent agreement with the stronger DET process occurring in device B than device A. Therefore, these experimental findings undoubtedly demonstrate the significant influence of the electroplex-emissive states on the occurrence of the RISC process and the effective DET channels from triplet excitons to triplet electroplexes in devices A and B.

Since the different mixing ratios between donor and acceptor in the donor:acceptor blend film as an emissive layer may modulate the EL spectra of devices with double-emissive states [8,30], we investigate the EL spectra of mCBP:Bphen- and mCBP:TPBi-based OLEDs with donor:acceptor mixing ratios of 1:4 and 4:1, namely, devices A1, A2, B1, and B2, as exhibited in Figs. S5(a) and S5(b) within the Supplemental Material [18], respectively. Compared with devices A and B with a donor:acceptor mixing ratio of 1:1, their normalized EL spectra just present slightly decreased exciton emissions. This is because, as the ratios of Bphen and TPBi acceptors increase or reduce, the distance between the donor and acceptor molecules increases compared with the case of a mixing ratio of 1:1. The increased molecular distance facilitates electroplex formation [25], which leads to weakened exciton emissions. On the other hand, as displayed in Figs. S6(a)–S6(d) within the Supplemental Material [18], the MEL traces of devices A1 and A2 show

an abnormal I -dependent RISC process, while the MEL traces of devices B1 and B2 present the conversion from ISC to RISC processes with increasing I . For devices A, A1, and A2, their EL spectra are always dominated by electroplex emissions, which lead to similar microscopic mechanisms in the devices. That is, these three devices present similar MEL line shapes induced by B -mediated RISC of the electroplex states. However, the EL spectra of devices B and B1 are dominated by exciton emissions, and the EL spectrum of device B2 is governed by electroplex emission. Although the main emission component of the EL spectrum changes in device B2, the occurrence intensities of these two emission states are similar, which results in the observed ISC process due to the superposition effects of the MEL traces. Therefore, the MEL traces of devices B, B1, and B2 show the conversion from B -mediated ISC to RISC processes with increasing I . As we can see, the I dependences, line shapes, and magnitude values of these MEL responses in devices A1, A2, B1, and B2 are analogous to those with a mixing ratio of 1:1, indicating the slight impact of the mixing ratios between donor and acceptor on the microscopic mechanisms of devices A and B.

E. Underlying physical microscopic processes occurring in devices A–C

Through a comparative analysis of our experimental data, as discussed in Sec. III D, we conclude that the observed RISC-governed MEL traces originate from the conversion from triplet to singlet electroplex states ($CT_1 \leftarrow CT_3$), but the underlying physical mechanisms in

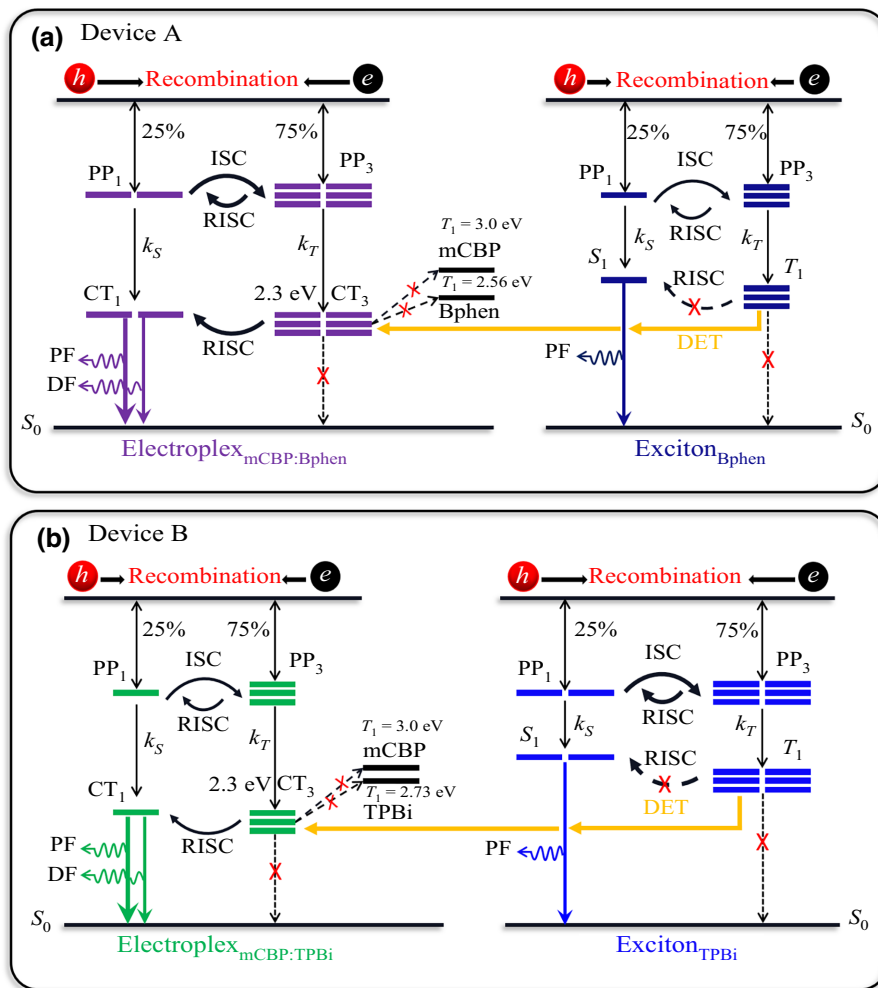


FIG. 5. Underlying physical microscopic processes in (a) device A and (b) device B.

coexisting electroplex and exciton devices need to be further investigated. Figures 5(a) and 5(b) exhibit schematic diagrams of excited-state formation and microscopic processes in devices A and B, respectively. When an external positive bias voltage is applied, the injected electrons and holes from the cathode and anode electrodes can move toward each other and recombine in the donor:acceptor blend layer [7]. Notably, some injected charge carriers can also recombine in the electron-transporting layer (ETL) of Bphen and TPBi for devices A and B due to the energy-level alignments shown in Figs. 1(a) and 1(b), respectively. Then, weakly bound singlet- and triplet-polaron pairs (PP_1 and PP_3) are formed in the donor:acceptor mixing layer [31] and on the ETL molecules in a ratio of 1:3, respectively. Sequentially, PP_1 and PP_3 in the mCBP:Bphen and mCBP:TPBi mixing layer in devices A and B will form weakly bound CT_1 and CT_3 states with rate constants of k_S and k_T or dissociate back into free carriers, but PP_1 and PP_3 on the ETL molecules in devices A and B can generate strongly bound singlet and triplet excitons (S_1

and T_1) with rate constants of k_S and k_T . Notably, PP_1 and PP_3 can transform into each other due to hyperfine interactions [32–34], and generally the ISC from PP_1 to PP_3 (PP ISC) is dominant in OLEDs, because a larger value of k_T than k_S (i.e., $k_T > k_S$) will induce a stronger ISC than RISC in polaron-pair states [35,36], and their related physical backgrounds are described in Text S2 within the Supplemental Material [18]. In addition, a large number of singlet states (S_1 , CT_1) can rapidly deactivate to the ground state (S_0) and produce prompt fluorescence (PF). Differently, for the Bphen and TPBi excitons in devices A and B, S_1 and T_1 cannot present the RISC process ($S_1 \leftarrow T_1$) due to their large energy barriers from T_1 to S_1 . Nevertheless, there are weak spin-exchange interactions and small energy differences between CT_1 and CT_3 because they are intrinsically intermolecular excited states [7,37] in the mCBP:Bphen and mCBP:TPBi mixing layers. Thus, CT_1 can be produced through the RISC process from CT_3 to CT_1 ($CT_1 \leftarrow CT_3$), leading to delayed fluorescence (DF). As reported in the literature [38–40], T_1 energies

of donor and acceptor should be high enough in high-efficiency exciplex- or electroplex-based OLEDs so that the energies of exciplexes and electroplexes can be well confined, and the CT RISC process can be significantly promoted. Therefore, the T_1 exciton energies of mCBP [$E(T_{1,\text{mCBP}}=3.0$ eV)] [41], Bphen [$E(T_{1,\text{Bphen}}=2.56$ eV)] [42], and TPBi [$E(T_{1,\text{TPBi}}=2.73$ eV)] [43] materials are given in Figs. 5(a) and 5(b). Clearly, $E(T_{1,\text{mCBP}})$ and $E(T_{1,\text{Bphen}})$ are higher than the CT_3 energy of the mCBP:Bphen electroplex [$E(\text{CT}_{3,\text{mCBP:Bphen}}=2.3$ eV), as calculated from the EL spectrum onset (535 nm)]. Similarly, $E(T_{1,\text{mCBP}})$ and $E(T_{1,\text{TPBi}})$ are also higher than the CT_3 energy of the mCBP:TPBi electroplex [$E(\text{CT}_{3,\text{mCBP:TPBi}}=2.3$ eV), as calculated from the EL spectrum onset (535 nm)]. As a result, these possible energy-loss channels ($\text{CT}_{3,\text{mCBP:Bphen}} \rightarrow T_{1,\text{mCBP}}$, $\text{CT}_{3,\text{mCBP:Bphen}} \rightarrow T_{1,\text{Bphen}}$, $\text{CT}_{3,\text{mCBP:TPBi}} \rightarrow T_{1,\text{mCBP}}$, and $\text{CT}_{3,\text{mCBP:TPBi}} \rightarrow T_{1,\text{TPBi}}$) can be effectively suppressed; thus, the strong CT RISC can exist in mCBP:Bphen and mCBP:TPBi electroplex states due to the complete confinement of CT_3 . Moreover, CT_3 states have a longer lifetime and a larger quantity than PP_1 states [29], causing the stronger CT RISC than the PP ISC in mCBP:Bphen and mCBP:TPBi electroplex states. It is worth mentioning that the DET channels ($T_{1,\text{Bphen}} \rightarrow \text{CT}_{3,\text{mCBP:Bphen}}$, $T_{1,\text{TPBi}} \rightarrow \text{CT}_{3,\text{mCBP:TPBi}}$) from triplet excitons to triplet electroplexes exist in devices A and B. Because DET usually refers to a short-range interaction between triplet excitons, it occurs from high-energy triplet excitons to low-energy ones [44,45]. Furthermore, DET can affect the evolutionary pathways of excited states and the optoelectronic performance of devices. Specifically, the occurrence of DET increases the number of CT_3 states from mCBP:Bphen and mCBP:TPBi, thereby facilitating the RISC processes from CT_3 to CT_1 in electroplex states and enhancing DF.

To explain the abundant behaviors of I -dependent MEL traces shown in Figs. 2(d)–2(f), I -dependent EL spectra of devices A–C at 300 K are shown in Figs. S3(a)–S3(c) within the Supplemental Material [18], respectively. As we can see, the normalized EL spectra of electroplex-dominated device A, exciton-dominated device B, and exciplex-only device C remain nearly constant with increasing I . This is probably because both electroplex and exciton components from devices A and B are enhanced at a certain ratio as I rises, leading to a fixed ratio of electroplex emission relative to exciton emission in devices A and B. Thus, we do not consider the relative changes in the emissive intensity of electroplexes and excitons when interpreting the rich I -dependent MEL curves of devices A and B. Factually, for devices A and B, at low current densities, the quantity of PP_3 as the precursor of excitons in the ETL is relatively small, and the quantity of T_1 generated from PP_3 is also small. Thus, the DET ($T_1 \rightarrow \text{CT}_3$) process is weak. Since the number of electroplexes is

greater than that of excitons in device A, and the amount of excitons is greater than that of electroplexes in device B [Figs. 2(a) and 2(b)], the MEL curves of devices A and B are determined by the microscopic processes of the electroplex_{mCBP:Bphen} (i.e., CT RISC-dominated MEL) and exciton_{TPBi} (i.e., PP ISC-governed MEL), respectively. This is because the MEL profiles of devices mainly depend on the superposition of B -sensitive microscopic processes, and ISC and RISC processes have opposite MEL responses [29]. Therefore, RISC and ISC processes can be observed in devices A and B at low current densities, respectively. As I rises, the number of PP_3 for the formation of excitons increases, further producing more T_1 . A large amount of CT_3 can be formed by the DET channels from T_1 , enhancing CT RISC of electroplexes. Consequently, the CT RISC channels in devices A and B increase with an increase of I , that is, an abnormal I -dependent RISC process is obtained in device A, whereas the conversion from ISC to RISC processes with increasing I can be observed in device B.

Figure S8 within the Supplemental Material [18] depicts a schematic diagram of the microscopic mechanisms in device C. As reported in the literature [29,42], there is an energy-leakage channel between the $\text{CT}_{3,m\text{-MTDATA:Bphen}}$ exciplex and $T_{1,\text{Bphen}}$ in device C because $E(T_{1,\text{Bphen}})$ is approximately equal to the CT_3 energy of the $m\text{-MTDATA:Bphen}$ exciplex [$E(\text{CT}_{3,m\text{-MTDATA:Bphen}}=2.52$ eV)]. This indicates that a large amount of $\text{CT}_{3,m\text{-MTDATA:Bphen}}$ is leaked, which weakens the CT RISC of exciplex states. Therefore, PP ISC is stronger than CT RISC in device C, and eventually the MEL curves of exciplex-only device C solely display the net ISC process because MEL in the exciplex-based device (device C) is an overlapping effect of the B -mediated ISC of polaron pairs and RISC of charge-transfer states, and ISC and RISC have opposite MEL curves. As depicted in Fig. S8 within the Supplemental Material [18], the energy gap between PP_1 and PP_3 is significantly smaller than that between CT_1 and CT_3 , but PP and CT states have similar magnetic field regions affecting these spin-conversion processes. The specific physical reasons for their similar characteristic magnetic fields can be found in Text S3 within the Supplemental Material [18]. Additionally, as I rises via elevating the device's bias voltage, the enlarged electric field in device C accelerates the dissociation of PP states and shortens the lifetime of PP states [26,46], causing the weakened PP ISC. Hence, the normal I -dependent ISC process, which is reduced with increasing I , is obtained in device C.

F. Temperature-dependent MEL responses of devices A–C

Generally, the mobility of charge carriers and the recombination rates of electron-hole pairs existing in OLEDs are dependent on the device's operational temperature [27,47].

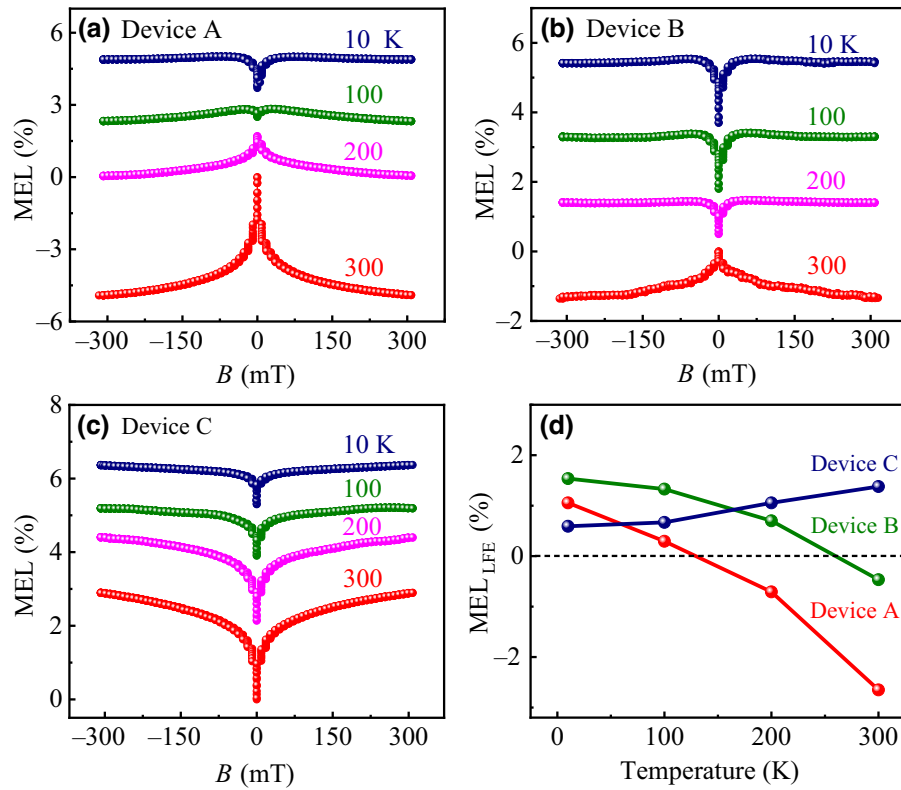


FIG. 6. Temperature-dependent MEL responses of (a) device A, (b) device B, and (c) device C at 100 μ A. (d) MEL_{LFE} values for devices A–C as a function of operational temperature.

We suppose this may result in remarkable temperature effects on the MEL behaviors of devices. Thus, we measure the temperature-dependent MEL responses of devices A–C at a fixed I (100 μ A), as shown in Figs. 6(a)–6(c), respectively. Intriguingly, as the operational temperature rises gradually from 10 to 300 K, the LFEs of MEL curves for devices A and B [Figs. 6(a) and 6(b)] show a conversion from ISC to RISC processes at different temperatures. For example, at 200 K, the LFE of device B still exhibits the ISC process, but the LFE of device A converts into the RISC process. This experimental result is consistent with the existence of a stronger RISC process occurring in device A than in device B at 300 K. According to the literature [37], the reason behind this conversion from ISC to RISC processes with increasing temperature is due to the endothermic characteristics of the RISC process. However, the LFEs of MEL traces from device C [Fig. 6(c)] reveal that the ISC process increases as the temperature increases from 10 to 300 K, which is the same as that of conventional exciton-type devices (for example, ITO/PEDOT:PSS/ N,N' -bis(naphthalen-1-yl)- N,N' -bis(phenyl)-benzidine (NPB)/tris(8-hydroxyquinolinato)aluminum (Alq_3)/LiF/Al) [48]. This temperature dependence can be explained by Onsager theory [26,46]. Specifically, the device voltage quickly increases at a low operational temperature, and the increased electric

field inside the device can enlarge the separation distance between electrons and holes in PP states, thereby enhancing the dissociation of PP states and shortening the lifetime of PP states. Thus, a weakened PP ISC process with decreasing temperature is obtained.

To quantitatively analyze the influence of operational temperatures on the occurrence probabilities of RISC and ISC processes, Fig. 6(d) depicts the MEL magnitudes of LFEs ($\text{MEL}_{\text{LFE}} = \text{MEL}_{B=9\text{mT}} - \text{MEL}_{B=0\text{mT}}$) as a function of operational temperatures for devices A–C. Obviously, the MEL_{LFE} values of devices A and B decrease with increasing temperature and even change from positive to negative, while the MEL_{LFE} value of device C monotonically rises with increasing temperature. These results directly reflect that the RISC processes in devices A and B and the ISC process in device C are synchronously enhanced with increasing operational temperature, which is better understood with the help of temperature-dependent EL measurements for devices A–C, as described in the following section.

G. Normalized temperature-dependent EL spectra of devices A–C

To further understand the physical behavior of temperature-dependent MEL traces from devices A–C

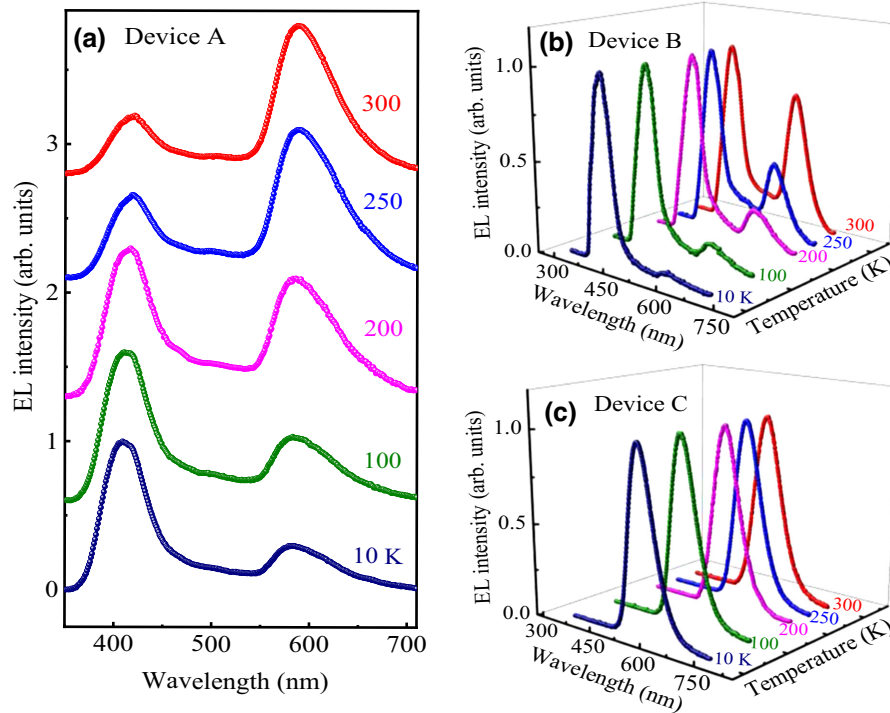


FIG. 7. Normalized temperature-dependent EL spectra of (a) device A, (b) device B, and (c) device C at 100 μA .

depicted in Figs. 6(a)–6(c), we measure their temperature-dependent EL spectra for devices A–C at $I = 100 \mu\text{A}$, as shown in Figs. 7(a)–7(c), respectively. It can be seen that the EL spectrum of device A gradually changes from electroplex domination at 300 K to exciton domination at low temperature. Although the EL spectrum of device B is always governed by exciton emissions, the electroplex is also weakened with decreasing temperature. The associated reasons behind these phenomena are closely dependent on the extended lifetime of the exciton compared with the electroplex and the reduced mobility of charge carriers on donor and acceptor molecules at low temperature. Their specific reasons are discussed in points (1) and (2). (1) As the device’s operational temperature decreases, both the lifetimes of exciton and electroplex states can be prolonged because of the reduced phonon thermal perturbation. However, the turn-on voltages of the devices simultaneously increase with decreasing temperature, which enhances the electric field inside the devices and accelerates the dissociation of the exciton and electroplex. Generally, an exciton is a strongly bound state, while an electroplex is a weakly bound state. Hence, the electroplex is more prone to dissociate into free charges than the exciton, and the exciton lifetime is much longer than the electroplex lifetime under the influence of an enhanced electric field within the device operating at low temperature. Consequently, the emission intensity of the

exciton has an obvious enhancement compared with that of the electroplex in devices A and B with decreasing temperature. (2) The room-temperature hole mobility of the mCBP donor is $1.1 \times 10^{-3} \text{ cm}^2 \text{ V}^{-1} \text{ s}^{-1}$ [49], and the room-temperature electron mobilities of the Bphen and TPBi acceptors are 5.2×10^{-4} and $3.3 \times 10^{-5} \text{ cm}^2 \text{ V}^{-1} \text{ s}^{-1}$ [50], respectively. That is, mCBP transports holes much easier than Bphen and TPBi transport electrons. Thus, with lower temperatures, the injected electrons in devices A and B are prone to stay in the LUMO levels of Bphen and TPBi, which causes stronger exciton emissions than electroplex emissions at low temperatures. The combined effects of (1) and (2) result in the experimental results of temperature-dependent EL variations of devices A and B depicted in Figs. 7(a) and 7(b). We mention above that the RISC process is mainly derived from electroplex states, but the ISC process originates from polaron pairs as the precursor of excitons. Therefore, the conversion from ISC to RISC processes with increasing temperature can be also explained by the temperature-dependent EL spectra of devices A and B. Differently, the EL spectrum of device C [Fig. 7(c)] has only one emission peak of an exciplex at different temperatures and barely varies with temperature; thus, the temperature-dependent MEL curves shown in Fig. 6(c) are independent of temperature-dependent EL spectra. These analyses demonstrate that the MEL curves are strongly correlated with the EL spectra of devices with

multiple emissive states, and changing the temperature is a feasible strategy to observe their physical behaviors.

IV. CONCLUSION

Here, to investigate the physical microscopic processes for electroplex-based devices, three kinds of donor:acceptor heterojunction OLEDs are fabricated: a coexisting electroplex and exciton but electroplex-dominated device, a coexisting electroplex and exciton but exciton-dominated device, and one pure exciplex-based device. Interestingly, via systematic room-temperature MEL measurements, we observe abundant unreported MEL behaviors: the abnormal I -dependent RISC process in the electroplex-dominated device, and the conversion from ISC to RISC processes with increasing I in the exciton-dominated device. This is attributed to the comprehensive effects of MEL curves, corresponding to exciton and electroplex emissions, and the DET channel from triplet excitons to triplet electroplexes. Combined with the MEL traces and the EL spectra of devices at various temperatures, the most vital finding is that the RISC process readily occurs in electroplex-based devices. By comparing the CT_3 energies of the exciplex and electroplex with the T_1 energies of various organic monomer materials, the specific reason is the effective energy confinement of triplet-electroplex states. In addition, these two coexisting electroplex and exciton devices present the conversion from ISC to RISC processes with increasing temperature, but the pure exciplex-based device shows only the normal temperature-dependent ISC process, which rises with increasing temperature. This conversion at low temperature can be explained by the increased exciton emissions as the temperature is reduced and by the endothermic property of the RISC process. On the whole, the selection of donor and acceptor materials has a significant impact on the occurrence of the RISC process, which will greatly affect the device's light-emission efficiency. Undoubtedly, this work not only deepens our understanding of the physical RISC process in coexisting electroplex and exciton devices but also provides ideas for designing highly efficient OLEDs using electroplex states.

ACKNOWLEDGMENTS

This work is supported by the National Natural Science Foundation of China (Grants No. 11874305 and No. 11374242).

[1] D. C. Chen, G. Z. Xie, X. Y. Cai, M. Liu, Y. Cao, and S. J. Su, Fluorescent organic planar pn heterojunction light-emitting diodes with simplified structure, extremely low driving voltage, and high efficiency, *Adv. Mater.* **28**, 239 (2016).

[2] M. Regnat, K. P. Pernstich, K.-H. Kim, J.-J. Kim, F. Nüesch, and B. Ruhstaller, Routes for efficiency enhancement in fluorescent TADF exciplex host OLEDs gained from an electro-optical device model, *Adv. Electron. Mater.* **6**, 1900804 (2020).

[3] J. H. Yun, J.-M. Kim, W. J. Chung, J. Lim, J. Y. Lee, Y. Lee, and C. Choo, A novel electroplex host with dual triplet exciton up-converting channels suppressing triplet exciton induced degradation mechanisms in blue organic light-emitting diodes, *J. Mater. Chem. C* **9**, 15242 (2021).

[4] X. Zhao, X. T. Tang, H. Q. Zhu, C. H. Ma, Y. Wang, S. N. Ye, L. Y. Tu, and Z. H. Xiong, Room-temperature observation for reverse intersystem crossing in exciplex-based OLEDs with balanced charge injection, *ACS Appl. Electron. Mater.* **3**, 3034 (2021).

[5] W.-Y. Hung, P.-Y. Chiang, S.-W. Lin, W.-C. Tang, Y.-T. Chen, S.-H. Liu, P.-T. Chou, Y.-T. Hung, and K.-T. Wong, Balance the carrier mobility to achieve high performance exciplex OLED using a triazine-based acceptor, *ACS Appl. Mater. Interfaces* **8**, 4811 (2016).

[6] K.-H. Kim, S.-J. Yoo, and J.-J. Kim, Boosting triplet harvest by reducing nonradiative transition of exciplex toward fluorescent organic light-emitting diodes with 100% internal quantum efficiency, *Chem. Mater.* **28**, 1936 (2016).

[7] Q.-S. Tian, X.-D. Zhu, and L.-S. Liao, Highly efficient exciplex-based OLEDs incorporating a novel electron donor, *Mater. Chem. Front.* **4**, 1648 (2020).

[8] M. X. Zhang, Z. J. Chen, L. X. Xiao, B. Qu, and Q. H. Gong, High-color-quality white top-emitting organic electroluminescent devices based on both exciton and electroplex emission, *Appl. Phys. Express* **4**, 082105 (2011).

[9] S. Y. Yang, X. L. Zhang, Y. B. Hou, Z. B. Deng, and X. R. Xu, Charge carriers at organic heterojunction interface: Exciplex emission or electroplex emission?, *J. Appl. Phys.* **101**, 096101 (2007).

[10] W. Song, J. Y. Lee, Y. J. Cho, H. Yu, H. Aziz, and K. M. Lee, Electroplex as a new concept of universal host for improved efficiency and lifetime in red, yellow, green, and blue phosphorescent organic light-emitting diodes, *Adv. Sci.* **5**, 1700608 (2018).

[11] M. Jung, K. H. Lee, J. Y. Lee, and T. Kim, A bipolar host based high triplet energy electroplex for an over 10 000 h lifetime in pure blue phosphorescent organic light-emitting diodes, *Mater. Horiz.* **7**, 559 (2020).

[12] Y. Tang, G. H. Xie, X. J. Yin, Y. H. Gao, J. Q. Ding, and C. L. Yang, Unravelling electroplex emission from long-range charge transfer based on a phosphorescent dendrimer as the electron donor, *J. Phys. Chem. Lett.* **11**, 5255 (2020).

[13] M. Y. Wei, G. Gui, Y.-H. Chung, L. X. Xiao, B. Qu, and Z. J. Chen, Micromechanism of electroplex formation, *Phys. Status Solidi B* **252**, 1711 (2015).

[14] C. X. Zhao, W. Y. Jia, K. X. Huang, Q. M. Zhang, X. H. Yang, and Z. H. Xiong, Anomalous temperature dependent magneto-conductance in organic light-emitting diodes with multiple emissive states, *Appl. Phys. Lett.* **107**, 023302 (2015).

[15] Y. F. Wang, K. Sahin-Tiras, N. J. Harmon, M. Wohlgenannt, and M. E. Flatté, Immense Magnetic Response of Exciplex Light Emission due to Correlated Spin-Charge Dynamics, *Phys. Rev. X* **6**, 011011 (2016).

- [16] Z. Y. Pang, D. L. Sun, C. Zhang, S. Baniya, O. Kwon, and Z. V. Vardeny, Manipulation of emission colors based on intrinsic and extrinsic magneto-electroluminescence from exciplex organic light-emitting diodes, *ACS Photonics* **4**, 1899 (2017).
- [17] J. Xu, X. T. Tang, X. Zhao, H. Q. Zhu, F. L. Qu, and Z. H. Xiong, Abnormal Reverse Intersystem Crossing of Polaron-Pair States and Its Conversion to Intersystem Crossing via the Regulation of Intermolecular Electron-Hole Spacing Distance, *Phys. Rev. Appl.* **14**, 024011 (2020).
- [18] See the Supplemental Material at <http://link.aps.org/supplemental/10.1103/PhysRevApplied.19.064055> for additional data descriptions of EQEs for devices A–C, EL spectra and MEL curves of devices A and B with different donor:acceptor mixing ratios, and microscopic mechanisms of exciplex formation.
- [19] S. A. Ying, Y. B. Wu, Q. Sun, Y. F. Dai, D. Z. Yang, X. F. Qiao, J. S. Chen, and D. G. Ma, High efficiency color-tunable organic light-emitting diodes with ultra-thin emissive layers in blue phosphor doped exciplex, *Appl. Phys. Lett.* **114**, 033501 (2019).
- [20] P. Chen, Q. M. Peng, L. Yao, N. Gao, and F. Li, Identifying the efficient inter-conversion between singlet and triplet charge-transfer states by magneto-electroluminescence study, *Appl. Phys. Lett.* **102**, 063301 (2013).
- [21] J. H. Seo, J. S. Park, S. J. Lee, B. M. Seo, K. H. Lee, J. K. Park, S. S. Yoon, and Y. K. Kim, Codoped spacer ratio effect on electroluminescence characteristics of hybrid white organic light-emitting diodes for reduced efficiency roll-off, *Jpn. J. Appl. Phys.* **49**, 090203 (2010).
- [22] Y. J. Cho, S. Taylor, and H. Aziz, Increased electromer formation and charge trapping in solution-processed versus vacuum-deposited small molecule host materials of organic light-emitting devices, *ACS Appl. Mater. Interfaces* **9**, 40564 (2017).
- [23] J. Chen, X. Zhao, X. T. Tang, Y. R. Ning, F. J. Wu, X. L. Chen, H. Q. Zhu, and Z. H. Xiong, An unprecedented spike of the electroluminescence turn-on transience from guest-doped OLEDs with strong electron-donating abilities of host carbazole groups, *Mater. Horiz.* **8**, 2785 (2021).
- [24] W. Jiang, G. M. Zhao, H. W. Chen, and Y. M. Sun, Novel ternary exciplex system based on TCTA dendrimer with a new linking type amongst various functional donors, *J. Mater. Sci.: Mater. Electron.* **33**, 11403 (2022).
- [25] D. Liu, A. Guo, Q. Y. Zhang, Y. L. Feng, G. M. Zhao, D. Y. Ma, H. W. Chen, W. Jiang, and Y. M. Sun, Spatial regulation of exciplex emission via dendritic molecular engineering, *J. Mater. Chem. C* **9**, 13347 (2021).
- [26] X. Zhao, J. Chen, X. T. Tang, F. J. Wu, Y. R. Ning, X. L. Chen, and Z. H. Xiong, Conversions from normal to abnormal current-dependent ISC and from abnormal to normal current-dependent RISC processes in exciplex-based OLEDs, *Adv. Mater. Interfaces* **9**, 2200155 (2022).
- [27] Y. Wang, Y. R. Ning, F. J. Wu, J. Chen, X. L. Chen, and Z. H. Xiong, Observation of reverse intersystem-crossing from the upper-level triplet to lowest singlet excitons ($T_2 \rightarrow S_1$) in tetra(*t*-butyl)rubrene-based OLEDs for enhanced light-emission, *Adv. Funct. Mater.* **32**, 2202882 (2022).
- [28] X. J. Zhan, Z. B. Wu, Y. B. Gong, J. Tu, Y. J. Xie, Q. Peng, D. G. Ma, Q. Q. Li, and Z. Li, Utilizing exciplex emission to achieve external quantum efficiency up to 18.1% in nondoped blue OLED, *Research* **2020**, 8649102 (2020).
- [29] F. J. Wu, X. Zhao, H. Q. Zhu, X. T. Tang, Y. R. Ning, J. Chen, X. L. Chen, and Z. H. Xiong, Identifying the exciplex-to-exciplex energy transfer in tricomponent exciplex-based OLEDs through magnetic field effect measurements, *ACS Photonics* **9**, 2713 (2022).
- [30] L. Gao, Z. X. Gao, K. X. Wang, Y. Q. Miao, Y. P. Zhao, W. Jia, Y. J. Zhou, H. Wang, and B. S. Xu, Ultra-simple two color WOLEDs with CRI exceeding 90 based on electron-transporting Bepp₂ simultaneously as blue emitter and exciplex acceptor, *J. Lumin.* **201**, 224 (2018).
- [31] W. Ratzke, S. Bange, and J. M. Lupton, Direct Detection of Singlet-Triplet Interconversion in OLED Magneto-Electroluminescence with a Metal-Free Fluorescence-Phosphorescence Dual Emitter, *Phys. Rev. Appl.* **9**, 054038 (2018).
- [32] T. Scharff, W. Ratzke, J. Zipfel, P. Klemm, S. Bange, and J. M. Lupton, Complete polarization of electronic spins in OLEDs, *Nat. Commun.* **12**, 2071 (2021).
- [33] P. Janssen, M. Cox, S. H. W. Wouters, M. Kemerink, M. M. Wienk, and B. Koopmans, Tuning organic magnetoresistance in polymer-fullerene blends by controlling spin reaction pathways, *Nat. Commun.* **4**, 2286 (2013).
- [34] R. Geng, R. C. Subedi, H. M. Luong, M. T. Pham, W. C. Huang, X. G. Li, K. Hong, M. Shao, K. Xiao, L. A. Hornak, and T. D. Nguyen, Effect of Charge Localization on the Effective Hyperfine Interaction in Organic Semiconducting Polymers, *Phys. Rev. Lett.* **120**, 086602 (2018).
- [35] S. A. Crooker, F. Liu, M. R. Kelley, N. J. D. Martinez, W. Nie, A. Mohite, I. H. Nayyar, S. Tretiak, D. L. Smith, and P. P. Ruden, Spectrally resolved hyperfine interactions between polaron and nuclear spins in organic light emitting diodes: Magneto-electroluminescence studies, *Appl. Phys. Lett.* **105**, 153304 (2014).
- [36] Y. Iwasaki, T. Osasa, M. Asahi, and M. Matsumura, Fractions of singlet and triplet excitons generated in organic light-emitting devices based on a polyphenylenevinylene derivative, *Phys. Rev. B* **74**, 195209 (2006).
- [37] K. Goushi, K. Yoshida, K. Sato, and C. Adachi, Organic light-emitting diodes employing efficient reverse intersystem crossing for triplet-to-singlet state conversion, *Nat. Photonics* **6**, 253 (2012).
- [38] W.-Y. Hung, G.-C. Fang, Y.-C. Chang, T.-Y. Kuo, P.-T. Chou, S.-W. Lin, and K.-T. Wong, Highly efficient bilayer interface exciplex for yellow organic light-emitting diode, *ACS Appl. Mater. Interfaces* **5**, 6826 (2013).
- [39] X.-K. Liu, Z. Chen, C.-J. Zheng, C.-L. Liu, C.-S. Lee, F. Li, X.-M. Ou, and X.-H. Zhang, Prediction and design of efficient exciplex emitters for high-efficiency, thermally activated delayed-fluorescence organic light-emitting diodes, *Adv. Mater.* **27**, 2378 (2015).
- [40] D. X. Luo, X.-L. Li, Y. Zhao, Y. Gao, and B. Q. Liu, High-performance blue molecular emitter-free and doping-free

- hybrid white organic light-emitting diodes: An alternative concept to manipulate charges and excitons based on exciplex and electroplex emission, *ACS Photonics* **4**, 1566 (2017).
- [41] H.-B. Kim and J.-J. Kim, Diffusion Mechanism of Exciplexes in Organic Optoelectronics, *Phys. Rev. Appl.* **13**, 024006 (2020).
- [42] L. P. Zhu, K. Xu, Y. P. Wang, J. S. Chen, and D. G. Ma, High efficiency yellow fluorescent organic light emitting diodes based on *m*-MTDATA/BPhen exciplex, *Front. Optoelectron.* **8**, 439 (2015).
- [43] V. Jankus, C.-J. Chiang, F. Dias, and A. P. Monkman, Deep blue exciplex organic light-emitting diodes with enhanced efficiency; *p*-type or *e*-type triplet conversion to singlet excitons?, *Adv. Mater.* **25**, 1455 (2013).
- [44] Y.-L. Chang, Z. B. Wang, M. G. Helander, J. Qiu, D. P. Puzzo, and Z. H. Lu, Enhancing the efficiency of simplified red phosphorescent organic light emitting diodes by exciton harvesting, *Org. Electron.* **13**, 925 (2012).
- [45] W. T. Xie, X. M. Peng, M. K. Li, W. D. Qiu, W. Li, Q. Gu, Y. H. Jiao, Z. J. Chen, Y. Y. Gan, K. K. Liu, and S.-J. Su, Blocking the energy loss of Dexter energy transfer in hyperfluorescence OLEDs via one-step phenyl-fluorene substitution of TADF assistant host, *Adv. Opt. Mater.* **10**, 2200665 (2022).
- [46] B. Hu and Y. Wu, Tuning magnetoresistance between positive and negative values in organic semiconductors, *Nat. Mater.* **6**, 985 (2007).
- [47] X. T. Tang, Y. Q. Hu, W. Y. Jia, R. H. Pan, J. Q. Deng, J. Q. Deng, Z. H. He, and Z. H. Xiong, Intersystem crossing and triplet fusion in singlet-fission-dominated rubrene-based OLEDs under high bias current, *ACS Appl. Mater. Interfaces* **10**, 1948 (2018).
- [48] P. Chen, Q. L. Song, W. C. H. Choy, B. F. Ding, Y. L. Liu, and Z. H. Xiong, A possible mechanism to tune magneto-electroluminescence in organic light-emitting diodes through adjusting the triplet exciton density, *Appl. Phys. Lett.* **99**, 143305 (2011).
- [49] K.-R. Wee, A.-L. Kim, S.-Y. Jeong, S. Kwon, and S. O. Kang, The relationship between the device performance and hole mobility of host materials in mixed host system for deep blue phosphorescent organic light emitting devices, *Org. Electron.* **12**, 1973 (2011).
- [50] J. W. Kim, S. I. Yoo, J. S. Kang, G. J. Yoon, S. E. Lee, Y. K. Kim, and W. Y. Kim, Quenching in single emissive white phosphorescent organic light-emitting devices, *Org. Electron.* **38**, 230 (2016).